Nanoscale

Cite this: *Nanoscale*, 2011, **3**, 4088

www.rsc.org/nanoscale

COMMUNICATION

6.5% efficient perovskite quantum-dot-sensitized solar cell†

Jeong-Hyeok Im, Chang-Ryul Lee, Jin-Wook Lee, Sang-Won Park and Nam-Gyu Park*

Received 19th July 2011, Accepted 15th August 2011
DOI: 10.1039/c1nr10867k

Highly efficient quantum-dot-sensitized solar cell is fabricated using *ca.* 2–3 nm sized perovskite $(CH_3NH_3)PbI_3$ nanocrystal. Spin-coating of the equimolar mixture of CH_3NH_3I and PbI_2 in γ-butyrolactone solution (perovskite precursor solution) leads to $(CH_3NH_3)PbI_3$ quantum dots (QDs) on nanocrystalline TiO_2 surface. By electrochemical junction with iodide/iodine based redox electrolyte, perovskite QD-sensitized 3.6 μm-thick TiO_2 film shows maximum external quantum efficiency (EQE) of 78.6% at 530 nm and solar-to-electrical conversion efficiency of 6.54% at AM 1.5G 1 sun intensity (100 mW cm^{-2}), which is by far the highest efficiency among the reported inorganic quantum dot sensitizers.

Introduction

Semiconductor quantum dots (QDs) have attracted considerable attention due to their unique opto-electronic properties.[1] Size tunable absorption,[2] high optical extinction coefficient[3] and multiple exciton generation[4] characteristics in semiconductor QDs are particularly suitable for light absorbers in solar cells. Three different QD solar cell configurations, a QD-arrayed *p-i-n* junction solar cell, a QD-sensitized solar cell and a QD-embedded polymer solar cell, were proposed,[5] where the QD-sensitized solar cell is an effective architecture to utilize QDs as absorbers because of using high surface area metal oxide supports for photosensitizing QDs. The QD-sensitized solar cell configuration is analogous to the dye-sensitized solar cell,[6] where the dye is replaced by QDs. Since the experimental verification of charge separation of photo-excited QD by n-type metal oxide and redox electrolyte,[7] numerous QD materials have been tested to confirm their photovoltaic performance in QD-sensitized solar cell structure [see Table 1 in ref. 8]. However, photovoltaic performance was mostly poor with conversion efficiency less than 1% at standard 1 sun illumination, until the report on CdS QD-sensitized solar cell with efficiency exceeding 1% in 2008.[9] Soon after, rapid progress has been made and, as a result, 4–5% efficiencies were recently achieved by using metal chalcogenides.[10]

Although metal chalcogenide QDs seem to be excellent inorganic sensitizers for QD-sensitized solar cells, recombination and chemical instability have been issued in ill-defined sulfur-based redox electrolyte.[11] To overcome such problems in metal chalcogenide QDs, lead iodide based perovskite-type sensitizers were recently introduced.[12] Perovskite $AB X_3$ (X = halogens) structure consists of organic components in cuboctahedral A site and inorganic components in octahedral B site and the chemistry of the organic and inorganic components can be tailored to tune the optical, electronic, magnetic, and mechanical properties of hybrid materials.[13] The $(CH_3NH_3)PbI_3$ perovskite used for sensitizer demonstrated solar-to-electrical energy conversion efficiency of 3.81% at 1 sun illumination in iodide-based redox electrolyte.[12] Despite excellent optical property of perovskite lead halide,[14] solution-based *in situ* deposition of $(CH_3NH_3)PbI_3$ perovskite sensitizer on TiO_2 surface led to maximum external quantum efficiency of about 50%,[12] which is, however, much lower than those of organometallic ruthenium dye and metal chalcogenide QDs. The low EQE from $(CH_3NH_3)PbI_3$ sensitizer is probably due to lack of detailed studies on its opto-electronic properties. Therefore, systematic and detailed investigations are required to get optimal performance from perovskite sensitizer.

In this paper, we report 6.54% efficient QD-sensitized solar cell based on perovskite $(CH_3NH_3)PbI_3$ sensitizer, which is, as far as we know, the highest efficiency among the reported inorganic QD sensitizers. Energy dispersive X-ray spectroscopy (EDS) and transmission electron microscopy (TEM) studies were performed to investigate 3-dimentional distribution of perovskite QD sensitizers in nanocrystalline TiO_2 film and adsorption of QD on TiO_2 surface. Effects of perovskite coating solution concentration and post-annealing temperature on photovoltaic performance were investigated. Electron transport and lifetime of perovskite QD-sensitized TiO_2 film were compared to those of a conventional ruthenium dye.

Experimental

$(CH_3NH_3)PbI_3$ was formed on TiO_2 surface from the γ-butyrolactone (Aldrich) solution containing equimolar mixture of CH_3NH_3I and PbI_2. CH_3NH_3I was synthesized by reacting 27.86 mL methylamine (40% in methanol, TCI) and 30 mL of hydroiodic acid (57 wt% in water, Aldrich) in 250 mL round bottomed flask at 0 °C for 2 h with stirring. The precipitate was recovered by evaporation at 50 °C for 1 h. The product, methyl ammonium iodide CH_3NH_3I, was washed with diethyl ether by stirring the solution for 30 min, which was repeated three times, and then finally dried at 60 °C in vacuum oven for 24 h. The synthesized CH_3NH_3I powder was mixed with PbI_2 (Aldrich) at 1 : 1 mol ratio in γ-butyrolactone at 60 °C for 12 h, followed by filtering twice using 13 mm diameter and 0.45 μm pore

School of Chemical Engineering and Department of Energy Science, Sungkyunkwan University, Suwon, 440-746, Korea. E-mail: npark@skku.edu; Fax: +82-31-290-7272; Tel: +82-31-290-7241

† Electronic supplementary information (ESI) available. See DOI: 10.1039/c1nr10867k

Table 1 Effect of annealing temperature on short-circuit photocurrent density (J_{SC}), open-circuit voltage (V_{OC}), fill factor (*FF*), and conversion efficiency (η) for the perovskite QD-sensitized solar cells. The 40.26 wt%. equimolar mixture of CH_3NH_3I and PbI_2 in γ-butyrolactone was used. The data were obtained under one sun illumination (100 mW cm^{-2}) at AM 1.5 G condition. The electrolyte composition was 0.9 M LiI, 0.45 M I_2, 0.5 M *t*BP and 0.05 M urea in ethyl acetate

Annealing temperature (°C)	TiO_2 film thickness (μm)	J_{SC} (mA cm^{-2})	V_{OC} (V)	*FF*	η (%)	Area (cm^2)
40	5.5	13.31	0.605	0.513	4.13	0.265
100		13.76	0.617	0.557	4.73	0.267
160		10.06	0.627	0.588	3.71	0.303

PVDF syringe filter (Whatman), which was used as a coating solution for *in situ* formation of $(CH_3NH_3)PbI_3$ on TiO_2 surface. The concentration of the equimolar mixture of CH_3NH_3I and PbI_2 was varied from 10.05 to 41.22 wt% (10.05, 20.13, 30.18, 40.26 and 41.22 wt%). For instance, 40.26 wt% solution contains 1.955g CH_3NH_3I (0.0123 mol) and 5.728 g PbI_2 (0.0123 mol) in 10 mL γ-butyrolactone (density = 1.14 g mL^{-1}).

20 nm sized crystalline TiO_2 particle-containing paste was prepared according to the method reported elsewhere.[15] FTO glasses (Pilkington, TEC-8, 8 Ω sq^{-1}) were cleaned in ethanol using an ultrasonic bath for 20 min. The FTO layer was first covered with 0.1 M Ti(IV) bis(ethyl acetoacetato)-diisopropoxide (Aldrich) in 1-butanol (Aldrich) solution by spin-coating method and this was heated at 500 °C for 15 min. The nanocrystalline TiO_2 paste was deposited on the pre-treated FTO substrate, which was followed by heating at 550 °C for 1 h. The thicknesses of the annealed TiO_2 films were determined by an alpha-step IQ surface profiler (KAL Tencor). The perovskite coating solution was spread on the annealed TiO_2 film (38.46 μL cm^{-2}) and was allowed to penetrate into the pores of the TiO_2 film for 1 min, which was spun for 40 s at speed of 2000 rpm in ambient atmosphere. The perovskite $(CH_3NH_3)PbI_3$ formed on TiO_2 surface was dried at different temperatures ranging form 40 °C to 160 °C for 30 min. Pt counter electrode was prepared by spreading a droplet of 7 mM $H_2PtCl_6 \cdot xH_2O$ in 2-propanol on a FTO substrate and heated at 400 °C for 20 min in air. The perovskite sensitizer-absorbed TiO_2 working electrode and the counter electrode were sandwiched using 25 μm thick Surlyn (SX1170-25, Solaronix). The redox electrolyte was prepared by dissolving 0.9 M LiI (Aldrich), 0.45 M I_2 (Aldrich), 0.5 M *tert*-butylpyridine *t*BP(Aldrich) 0.05 M urea (Aldrich) in ethyl acetate (Aldrich), which was introduced into the space of the sealed electrodes prior to measurement.

X-ray diffraction (XRD) analysis was performed on a Rigaku D/MAX 2400 diffractometer using Cu Ka radiation at scan rate of 4 °C min^{-1} under operation condition of 30 kV and 40 mA. For XRD measurement, $(CH_3NH_3)PbI_3$ powder was obtained by drying the solution contained CH_3NH_3I and PbI_2 at 100 °C. The absorbance of the $(CH_3NH_3)PbI_3$ adsorbed on TiO_2 film was recorded by a UV-vis spectrophotometer (Agilent 8453) in the wavelength ranging from 300 to 1000 nm.

Distribution of perovskite $(CH_3NH_3)PbI_3$ in TiO_2 film was investigated using a distribution mapping technique by energy dispersive X-ray spectroscope (EDS) combined with a field-emission scanning electron microscope (FE-SEM, Jeol JSM 6700F). X-ray energies corresponding to Ti, Pb and I were collected as the SEM scanned the electron beam over the surface and cross-sectional area in TiO_2 film. The X-ray data was synchronized with the SEM image and an 'element image' was created showing the presence of the selected element throughout the selected area. TEM images were investigated using a high-resolution transmission electron microscope (HR-TEM, Jeol, JEM-2100F) at an acceleration voltage of 200 kV. Photocurrent and voltage were measured from a solar simulator equipped with 450 W Xenon lamp (Newport 6279NS) and a Keithley 2400 source meter. Light intensity was adjusted with the NREL-calibrated Si solar cell having KG-2 filter for approximating one sun light intensity (100 mW cm^{-2}). While measuring current and voltage, the cell was covered with a black mask having an aperture,[16] where the aperture area was slightly smaller than the active area. External quantum efficiency (EQE) was measured using a specially designed EQE system for dye-sensitized solar cell (PV measurement, Inc.). A 75W Xenon lamp was used as a light source for generating monochromatic beam. Calibration was accomplished using a silicon photodiode, which was calibrated using the NIST-calibrated photodiode G425 as a standard. EQE data were collected at DC mode. Thermogravimetric analysis of $(CH_3NH_3)PbI_3$ was performed at rate of 10 °C min^{-1} from ambient temperature to 500 °C under air by using a TG/DTA setup (SEICO Ins. 6000). Differential scanning calorimeter of $(CH_3NH_3)PbI_3$ was performed at rate of 10 °C min^{-1} from 22 °C to 320 °C under air by using a DSC setup (SEICO Ins. DSC6100).

The time constants for transport and recombination of the photo-injected electrons were measured by using a photocurrent and photovoltage transient setup. The cells were probed with a weak laser pulse at 532 nm superimposed on a relatively large, back ground (bias) illumination at 680 nm. The bias light was illuminated by a 0.5 W diode laser (B&W TEK Inc., Model: BWF1-670-300E/55370). The intensity of the light was adjusted using ND filters (neutral density filters). The 680 nm bias light is only weakly absorbed by the dye, and therefore the injected electrons are introduced into a narrow spatial region of the film, corresponding to where the probe light enters the film. A 30 mW frequency-doubled Nd:YAG laser (Laser-Export Co. Ltd. Model: LCS-DTL-314QT) (λ = 532 nm, pulse duration 10ns) was used as probe light. The photocurrent transients were obtained by using a Stanford Research Systems model SR570 low-noise current preamplifier, amplified by a Stanford Research Systems model SR 560 low-noise preamplifier, and recorded on Tektronics TDS 3054B digital phosphore oscilloscope 500 MHz 5GS s^{-1} DPO. The photovoltage transients were obtained by using SR560 preamplifier, which was recorded on oscilloscope combined with Keithley 2400 measure unit. The photocurrent- and the photovoltage-time curves were fitted with an exponential relationship, $y(t) = \exp(-t/\tau)$, where y represents photocurrent density or photovoltage, t is time and τ (τ_C for electron transport and τ_R for recombination) is constant.

Results and discussion

$(CH_3NH_3)PbI_3$ formed from an equimolar mixture of CH_3NH_3I and PbI_2 in γ-butyrolactone is crystallized as tetragonal perovskite

structure with lattice parameters of a = b = 8.883 Å and c = 12.677 Å, which is confirmed by XRD pattern (Figure S1(a)†). The structure of the synthesized perovskite $(CH_3NH_3)PbI_3$ is well consistent with the previous report.[17] *In situ* formation of perovskite $(CH_3NH_3)PbI_3$ on TiO_2 surface is also confirmed by XRD pattern (Figure S1(b)†). The sharp X-ray diffraction peak of the as-prepared $(CH_3NH_3)PbI_3$ is broadened after deposition onto TiO_2 surface, which underlines that the size of perovskite $(CH_3NH_3)PbI_3$ is reduced. Fig. 1 shows surface and cross-sectional EDS mapping, where Pb and I are well distributed three-dimensionally in the mesoporous TiO_2 film. Weight percentages from EDS elemental analysis of the film surface are found to be 2.58%, 38.36%, 50.18%, 5.70% and 3.18% for C, O, Ti, I and Pb, respectively, which corresponds to 5.78%, 64.44%, 28.16%, 1.21% and 0.41% in atomic percentage. This indicates that the ratio of Pb to I is 1 : 3. Compared to the Ti atomic %, relatively lower atomic percentage of lead indicates that the perovskite sensitizer is not densely covered on TiO_2 surface.

Fig. 2 shows high resolution TEM micrographs of perovskite $(CH_3NH_3)PbI_3$ deposited TiO_2 nanoparticle, along with pure $(CH_3NH_3)PbI_3$ particles obtained by drying the γ-butyrolactone solution and bare TiO_2 nanoparticles. The perovskite $(CH_3NH_3)PbI_3$ are distributed homogeneously on the surface of TiO_2 nanoparticles as can be seen in Fig. 2(a). It is noted that shapeless nanocrystalline $(CH_3NH_3)PbI_3$ with more than 10 nm (Fig. 2(c)) is surprisingly changed to semi-spheres with average diameter of about 2.5 nm when it is deposited on TiO_2 surface (Fig. 2(b)), which indicates that smaller quantum dot is energetically favorable on TiO_2 surface. Moreover,

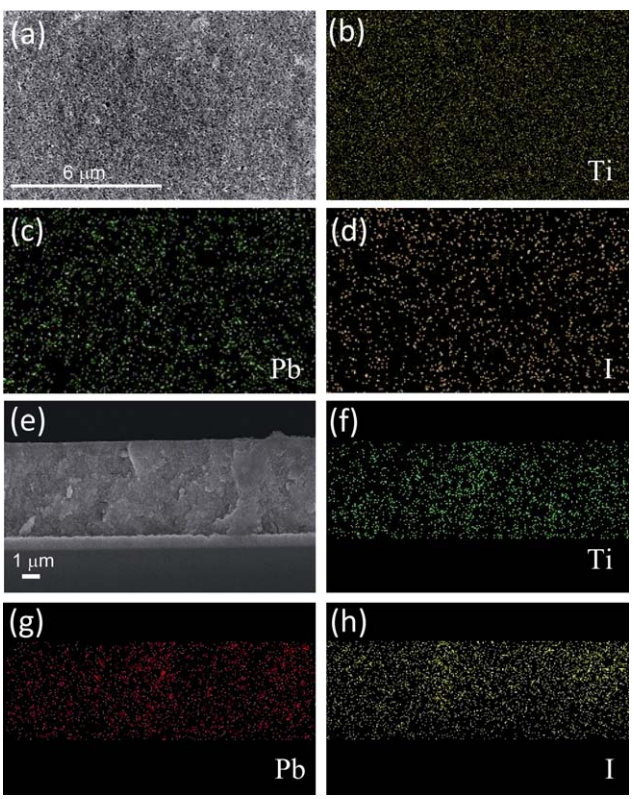

Fig. 1 (a) Plan view of SEM micrographs of $(CH_3NH_3)PbI_3$ deposited TiO_2 film and EDS mapping of (b) titanium, (c) lead and (d) iodine. (e) Cross-sectional SEM micrographs of $(CH_3NH_3)PbI_3$ deposited TiO_2 film and EDS maps of (f) titanium, (g) lead and (h) iodine.

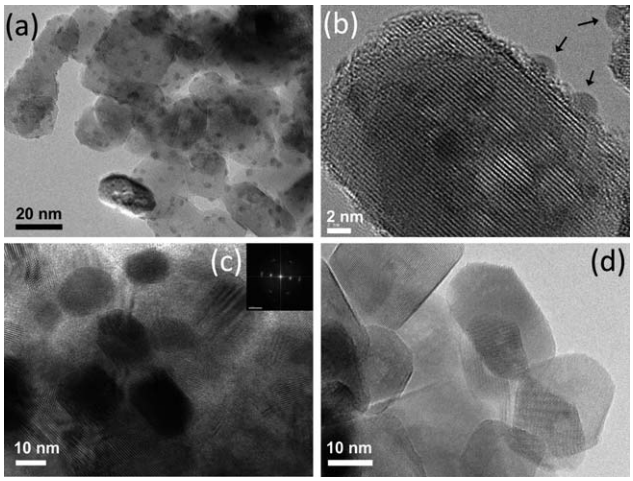

Fig. 2 TEM micrographs of (a) wide view of $(CH_3NH_3)PbI_3$ deposited TiO_2, (b) magnified image of $(CH_3NH_3)PbI_3$ deposited TiO_2, (c) pure $(CH_3NH_3)PbI_3$ and (d) bare TiO_2. Arrows in (b) indicates quantum dot perovskite $(CH_3NH_3)PbI_3$ with semi-spherical shape. Inset in (c) shows selected area electron diffraction pattern of pure $(CH_3NH_3)PbI_3$. For the (a) and (b) TEM images, 30.18 wt% and 40.26 wt% perovskite precursor solution were used, respectively.

perovskite QDs are sparsely adsorbed on TiO_2 surface as can be seen from the wide view of TEM in Fig. 2(a), which is consistent with the EDS elemental analysis. Number of QDs deposited on TiO_2 surface is estimated to be about 3.5×10^4 μm^{-2} from number of QDs in a Gaussian box of TEM image (Figure S2†), which is corresponding to *ca.* 18 particles per one TiO_2 particle surface by assuming that TiO_2 particle is sphere with diameter of 20 nm.

With increasing concentration (weight %) of the equimolar mixture of CH_3NH_3I and PbI_2 solution for *in situ* formation of perovskite $(CH_3NH_3)PbI_3$ QDs on TiO_2 surface, the color is changed from yellow (10.05 wt%) to black (40.26 wt%) (Fig. 3(a)), which may be due to a quantum size effect and/or an increased density of QDs. UV-vis absorption spectra in Fig. 3(b) show that absorption intensity and absorption onset wavelength increase simultaneously as the concentration increases, which is attributed to color change of QD-deposited TiO_2 film. As can be seen in Fig. 3(c), photovoltaic performance is significantly influenced by the perovskite precursor solution concentration. For the given TiO_2 thickness of about 5.5 μm, photocurrent density (J_{SC}) increases from 0.88 to 3.53, 8.12 and 13.31 mA cm^{-2} as the concentration increases from 10.05 to 20.13, 30.18 and 40.26 wt%, respectively. Open-circuit voltage (V_{OC}) is also slightly improved from 0.548 to 0.584, 0.591 and 0.605 V, which is due to the increased photocurrent density according to the relation of $V_{OC} = (kT/q)[\ln(I_L/I_0) + 1]$, where k, T, q, I_L and I_0 represent Boltzmann constant, temperature, electron charge, photocurrent and reverse saturation current, respectively. It cannot be ruled out that the increased voltage is partly due to reduction of recombination by the increased QD coverage. As a result, overall conversion efficiency is improved from 0.32% to 1.38%, 2.96% and 4.13%. Strong enhancement of EQE is observed at around 500 nm as increasing the concentration up to 30.18 wt% and further improvement at longer wavelength is realized when increasing the concentration from 30.18 to 40.26 wt% as can be seen in Fig. 3(d). The increased photocurrent and EQE are likely to be related to the change of absorption characteristics (the increased absorption magnitude and/or the shift of its

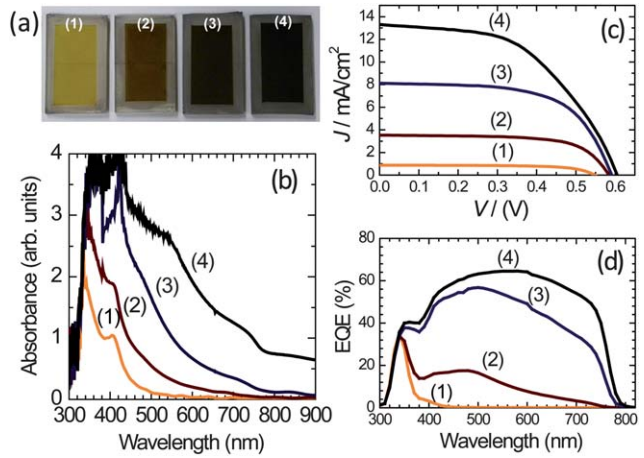

Fig. 3 (a) The perovskite $(CH_3NH_3)PbI_3$ QD-sensitized 5.5 μm thick TiO_2 films depending on concentration of the equimolar mixture of CH_3NH_3I and PbI_2 in in γ-butyrolactone (perovskite QD precursor solution), where (1), (2), (3) and (4) were obtained by deposition of 10.05, 20.13, 30.18 and 40.26 wt% solution, respectively, (b) UV-vis absorption spectra of 1.4 μm thick TiO_2 films depending on the concentration of perovskite QD precursor solution, (c) photocurrent–voltage curves and (d) external quantum efficiency (EQE) of 5.5 μm thick QD-sensitized TiO_2 films depending on the concentration of perovskite QD precursor solution. $(CH_3NH_3)PbI_3$ coated TiO_2 films were dried at 40 °C for 30 min.

onset to longer wavelength) as observed in UV-vis spectra in Fig. 3 (b). Similar observation was reported previously for the case of CdSe QD-sensitized solar cell,[10b] where increase of absorption magnitude and red shift of its onset were detected when increasing CdSe coating cycle. It was also observed that the EQE intensity gradually increased and the absorption onset in EQE spectra shifted to longer wavelengths, which is obviously due to quantum size effect, associated with change of band gap. However, our case is somewhat different from the CdSe result. When comparing UV-vis absorption spectra with EQE, except for the 10.05 wt%, the absorption onset in EQE is almost identical regardless of change in concentration. This indicates that bandgap of perovskite QD is not significantly altered by the change of concentration of the perovskite precursor solution. According to the detailed investigation for the size of QDs deposited TiO_2 particles depending on concentration of the perovskite precursor solution (Figure S3†), *ca.* 2.5 nm sized perovskite QD hardly changed with concentration. Thus the increased EQE with increasing the concentration is more closely related to the enhancement of optical absorption.

Effect of temperature on photovoltaic performance is investigated. Based on the thermal stability of perovskite QD upto 300 °C as confirmed by thermogravimetric analysis measurement (Figure S4†), photovoltaic performance is compared by changing the annealing temperature of the perovskite QD-sensitized TiO_2 film from 40 °C to 160 °C for 30 min. The annealing temperature can alter photovoltaic property to some extent (Figures S5 (a) and (b)†), where photocurrent of 13.31 mA cm^{-2}, voltage of 0.6046 V and fill factor of 0.513 for a 40 °C-dried QD-sensitized *ca.* 5.5 μm thick TiO_2 layer are slightly improved to 13.76 mA cm^{-2}, 0.6172 V and 0.557 upon increasing the annealing temperature to 100 °C (Table 1). As a result, conversion efficiency is improved by about 14.5%. On the other hand, further increase in the annealing temperature from 100 °C to 160 °C diminishes the efficiency from 4.73% to 3.71%, which is mainly due to the lowered photocurrent density. EQE spectra (Figure S5 (b)†) show that the decreased photocurrent density at high temperature treatment such as 160 °C is attributed to a significant loss in EQE at long wavelength region (above 500 nm). The EQE spectral feature of 160 °C post-treatment looks similar to the EQE spectrum corresponding to 30.18 wt% in Fig. 3(c). The UV-vis spectra depending on the annealing temperature show that the absorption magnitude increases as temperature increases from 40 °C to 100 °C, whereas it decreases significantly when temperature is elevated to 160 °C (Figure S6†). Finally, we investigate TiO_2 film thickness effect, where the concentration is optimized to 41.22 wt% by considering solubility limit of equimolar mixture of CH_3NH_3I and PbI_2. Photovoltaic property is found to be significantly influenced by TiO_2 film thickness (Figures S5 (c) and (d)†), in which a TiO_2 layer thinner than 5.5 μm (so far, concentration and temperature effects were studied with this film thickness) shows better photocurrent density and EQE, whereas, a thicker layer shows worse performance (Table 2). A 6.2% efficient perovskite QD-sensitized TiO_2 layer is achieved from optimizing TiO_2 film thickness.

Fig. 4 (a) and (b) compares the photovoltaic performance between perovskite QD and a conventional ruthenium-based organometallic N719 dye, and photovoltaic parameters are listed in Table 3. For relative comparison analysis, TiO_2 film thickness is adjusted to 3.6 μm and the same redox electrolyte is used. A 41.22 wt% coating solution is used for perovskite QD deposition. Photocurrent density of the perovskite QD-sensitized cell (~16 mA cm^{-2}) is almost two times higher than that of the N719-sensitized one (~9 mA cm^{-2}). From transmittance data for QD-deposited and N719-adsorbed thin films, absorption coefficients are estimated to be 1.5×10^4 cm^{-1} at 550 nm and 1.5×10^3 cm^{-1} at 540 nm for perovskite QD and N719, respectively, which indicates that absorption coefficient of perovskite QD is an order of magnitude higher than that of N719 (Fig. 4 (c) and (d)). In addition, higher absorption coefficient requires thinner film, associated with reciprocal absorption coefficient. For this reason, at given thin TiO_2 layer, perovskite QD shows much higher photocurrent density than N719. Reciprocal absorption coefficient for perovskite QD is estimated to be about 0.7 μm at 580 nm and 2 μm at

Table 2 Effect of TiO_2 film thickness on short-circuit photocurrent density (J_{SC}), open-circuit voltage (V_{OC}), fill factor (*FF*), and conversion efficiency (η) for the perovskite QD-sensitized solar cells. The 41.22 wt%. equimolar mixture of CH_3NH_3I and PbI_2 in γ-butyrolactone was used. The data were obtained under one sun illumination (100 mW cm^{-2}) at AM 1.5 G condition. The electrolyte composition was 0.9 M LiI, 0.45 M I_2, 0.5 M *t*BP and 0.05 M urea in ethyl acetate

TiO_2 film thickness (μm)	J_{SC} (mA cm^{-2})	V_{OC} (V)	*FF*	η (%)	Area (cm^2)
3.6	15.99	0.629	0.617	6.20	0.309
5.5	14.31	0.616	0.589	5.19	0.284
8.6	10.15	0.559	0.594	3.37	0.277

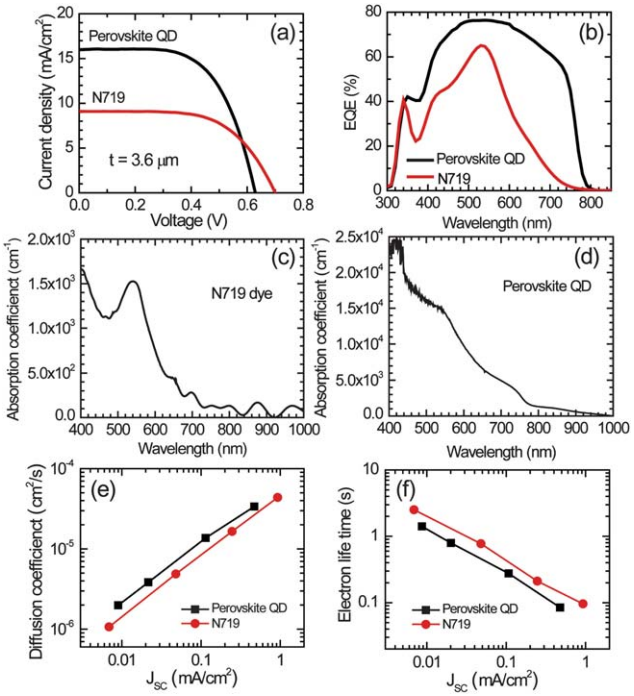

Fig. 4 Comparison of (a) photocurrent–voltage, (b) EQE, (c, d) absorption coefficients, (e) electron diffusion coefficient and (f) electron lifetime of perovskite QD-sensitized solar cell and N719 dye-sensitized solar cell. A 41.22 wt% equimolar mixture of CH_3NH_3I and PbI_2 in γ-butyrolactone was used for deposition of perovskite QD. The deposited film was annealed at 100 °C for 30 min. N719 dye was adsorbed on TiO_2 surface by dipping the TiO_2 film in 0.5 mM N179 ethanol solution for 4 h at 40 °C. For relative comparison analysis, TiO_2 film thickness was fixed to be 3.6 μm and the same electrolyte, comprising 0.9 M LiI, 0.45 M I_2, 0.5 M tBP and 0.05 M urea in ethyl acetate, was used. Absorption coefficients of (c) N719 dye and (d) perovskite $(CH_3NH_3)PbI_3$ QD were calculated from $T = I/I_0 = \exp(-\alpha l)$, where T, I, I_0, α and l represent transmittance, transmitted light intensity, incident light intensity, absorption coefficient and TiO_2 film thickness (2.3 μm for N719 and 1.4 μm for perovskite QD), respectively. Electron diffusion coefficient (D_n) was calculated from $2.35 \times \tau_c \times D_n = d^2$, where τ_c and d represent time constant for electron transport and TiO_2 film thickness, respectively.

800 nm, which is indicative of short penetration depth and supports the higher photocurrent density at thinner TiO_2 film.

Fig. 4 (e) and (f) compare electron transport rate and electron lifetime, where electron transport in perovskite QD-sensitized TiO_2 is found to be slightly faster than that in N719-sensitized one, whereas electron lifetime is slightly shorter for QD-sensitized layer than for N719-sensitized one. The higher electron diffusion coefficient in the TiO_2 layer sensitized with perovskite QDs is likely to be due to more

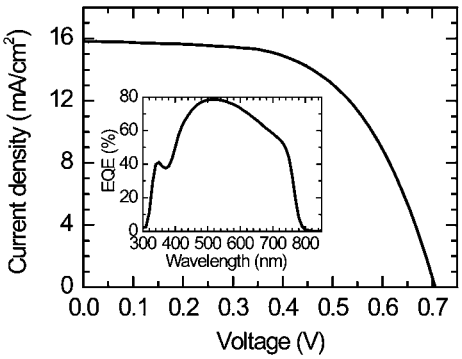

Fig. 5 Photocurrent–voltage curve and EQE for the perovskite $(CH_3NH_3)PbI_3$ QD-sensitized TiO_2 film whose surface was modified with $Pb(NO_3)_2$. Thickness of TiO_2 film was 3.6 μm and the redox electrolyte used was composed of 0.9 M LiI, 0.45 M I_2, 0.5 M *tert*-butylpyridine and 0.05 M urea in ethyl acetate.

photo-injected electrons, where the diffusion coefficient has been reported to be proportional to the photo injected electron density.[18] The difference in electron lifetime is probably related to difference in sensitizer coverage fraction on TiO_2 surface. As observed from EDS and TEM, bare TiO_2 surface exposed directly to electrolyte can be found more in QD-sensitized film than in N719-sensitized one, which is likely to accelerate electron recombination. Since the decrease in electron lifetime is mostly compensated by the improved electron transport rate, charge collection efficiency of perovskite QD-sensitized layer is similar to that of N719-sensitized one, where charge collection efficiency is found to reach 98% for the perovskite QD-sensitized solar cell. Further improvement has been achieved by surface modification of TiO_2 with $Pb(NO_3)_2$ prior to deposition of perovskite QD, in which conversion efficiency is improved from 6.2% to 6.54% ($J_{SC} = 15.82$ mA cm^{-2}, $V_{OC} = 0.706$ V and $FF = 0.586$) due to the increased V_{OC} (Fig. 5). The large increase in voltage suggests reduction of recombination after coating TiO_2 with $Pb(NO_3)_2$, which indicates that the $Pb(NO_3)_2$ probably acts as blocking layer. As a result, the maximum EQE shows 78.6% at 530 nm that approaches almost 100% after correction by 20% light reflection at FTO-coated glass substrate.

Conclusion

In conclusion, we demonstrated highly efficient QD-sensitized solar cell based on perovskite $(CH_3NH_3)PbI_3$. Studies on TiO_2 film thickness effect showed that thinner film had higher photocurrent density compared to relatively thicker layer due to high absorption coefficient of perovskite QD, one order of magnitude higher than the absorption coefficient of N719 dye. From the detailed investigation

Table 3 Comparison of photovoltaic performance of perovskite QD-sensitized solar cell and N719 dye-sensitized solar cells. For deposition of perovskite QD on TiO_2 surface, a 41.22 wt% coating solution was used and the deposited film was annealed at 100 °C for 30 min. N719 dye was adsorbed on TiO_2 surface by dipping the TiO_2 film in 0.5 mM N179 ethanol solution for 4 h at 40 °C. For relative comparison analysis, TiO_2 film thickness was fixed to be 3.6 μm and the same electrolyte, comprising 0.9 M LiI, 0.45 M I_2, 0.5 M *t*BP and 0.05 M urea in ethyl acetate, was used. The data were obtained under one sun illumination (100 mW cm^{-2}) at AM 1.5 G condition

Sensitizer	J_{SC} (mA cm^{-2})	V_{OC} (V)	*FF*	η (%)	Area (cm^2)
Perovskite QD	15.99	0.629	0.617	6.20	0.309
N 719	9.10	0.700	0.611	3.89	0.377

on perovskite coating solution concentration, post-annealing condition and TiO_2 surface modification, the best efficiency of 6.54% was obtained at AM 1.5G 1 sun illumination, which is by far the highest efficiency among the reported QD-sensitized solar cells. It is necessary to mention, however, that the stability of the perovskite (CH_3NH_3)PbI_3 QD-sensitized solar cell under continued irradiation is approximately 10 min (about 80% degradation) because QD tends to be dissolved gradually into the redox electrolyte. Studies to improve long-term stability are under way.

Acknowledgements

This work was supported by the National Research Foundation of Korea (NRF) grant funded by the Ministry of Education, Science and Technology (MEST) of Korea under contracts No. 2010-0014992, 2010-0028821, 2010-0001842 (ERC program) and R31-2008-10029 (WCU program) and the Korea Institute of Energy Technology Evaluation and planning (KETEP) grant funded by the Ministry of Knowledge Economy under contract No. 20103020010010. We are grateful to Prof. C.W. Yang for discussion on TEM measurements.

References

1 (*a*) E. H. Sargent, *Nat. Photonics*, 2009, **3**, 325–331; (*b*) K.-S. Cho, E. K. Lee, W.-J. Joo, E. Jang, T.-H. Kim, S. J. Lee, S.-J. Kwon, J. Y. Han, B.-K. Kim, B. L. Choi and J. M. Kim, *Nat. Photonics*, 2009, **3**, 341–345; (*c*) A. L. Rogach, T. Franzl, T. A. Klar, J. N. Gaponik, V. Lesnyak, A. Shavel, A. Eychmüller, Y. P. Rakovich and J. F. Donegan, *J. Phys. Chem. C*, 2007, **111**, 14628–14637.

2 (*a*) T. Takagahara and K. Takeda, *Phys. Rev. B: Condens. Matter*, 1992, **46**, 15578–15581; (*b*) S. Kan, T. Mokari, E. Rothenberg and U. Banin, *Nat. Mater.*, 2003, **2**, 155–158; (*c*) C. A. Leatherdale, W.-K. Woo, F. V. Mikulec and M. G. Bawendi, *J. Phys. Chem. B*, 2002, **106**, 7619–7622.

3 (*a*) W. Yu, L. Qu, W. Guo and X. Peng, *Chem. Mater.*, 2003, **15**, 2854–2860; (*b*) A. J. Nozik, *Nat. Nanotechnol.*, 2009, **4**, 548–549.

4 A. J. Nozik, *Phys. E.*, 2002, **14**, 115–120.

5 B. O′Regan and M. Grätzel, *Nature*, 1991, **353**, 737–739.

6 R. Vogel, K. Pohl and H. Weller, *Chem. Phys. Lett.*, 1990, **174**, 241–246.

7 (*a*) D. Liu and P. V. Kamat, *J. Phys. Chem.*, 1993, **97**, 10769–10773; (*b*) R. Vogel, P. Hoyer and H. Weller, *J. Phys. Chem.*, 1994, **98**, 3183–3188; (*c*) A. Zaban, O. I. Micic, B. A. Gregg and A. J. Nozik, *Langmuir*, 1998, **14**, 3153–3156.

8 S. Rühle, M. Shalom and A. Zaban, *ChemPhysChem*, 2010, **11**, 2290–2304.

9 H. J. Lee, J.-H. Yum, H. C. Leventis, S. M. Zakeeruddin, S. A. Haque, P. Chen, S. I. Seok, M. Grätzel and M. K. Nazeeruddin, *J. Phys. Chem. C*, 2008, **112**, 11600–11608.

10 (*a*) Y.-L. Lee and Y.-S. Lo, *Adv. Funct. Mater.*, 2009, **19**, 604–609; (*b*) V. Gonzalez-Pedro, X. Xu, I. Mora-Sero and J. Bisquert, *ACS Nano*, 2010, **4**, 5783–5790; (*c*) J. A. Chang, J. H. Rhee, S. H. Im, Y. H. Lee, H.-J. Kim, S. I. Seok, M. K. Nazeeruddin and M. Grätzel, *Nano Lett.*, 2010, **10**, 2609–2612; (*d*) X.-Y. Yu, B.-X. Lei, D.-B. Kuang and C.-Y. Su, *Chem. Sci.*, 2011, **2**, 1396–1400.

11 G. Hodes, *J. Phys. Chem. C*, 2008, **112**, 17778–17787.

12 A. Kojima, K. Teshima, Y. Shirai and T. Miyasaka, *J. Am. Chem. Soc.*, 2009, **131**, 6050–6051.

13 (*a*) D. B. Mitzi, C. A. Feild, W. T. A. Harrison and A. M. Guloy, *Nature*, 1994, **369**, 467–469; (*b*) C. R. Kagan, D. B. Mitzi and C. D. Dimitrakopoulos, *Science*, 1999, **286**, 945–947; (*c*) D. B. Mitzi, *Prog. Inorg. Chem.*, 1999, **48**, 1–121.

14 (*a*) G. C. Papavassiliou, *Mol. Cryst. Liq. Cryst.*, 1996, **286**, 231–238; (*b*) K. Tanaka, T. Takahashi, T. Ban, T. Kondo, K. Uchida and N. Miura, *Solid State Commun.*, 2003, **127**, 619–623; (*c*) K. Yamada, H. Kawaguchi, T. Matsui, T. Okuda and S. Ichiba, *Bull. Chem. Soc. Jpn.*, 1990, **63**, 2521–2525.

15 M.-J. Kim, C.-R. Lee, W.-S. Jeong, J.-H. Im, T. I. Ryu and N.-G. Park, *J. Phys. Chem. C*, 2010, **114**, 19849–19852.

16 (*a*) J. H. Park, H.-J. Koo, B. J. Yoo, K. C. Yoo, K. G. Kim, W. Y. Choi and N.-G. Park, *Sol. Energy Mater. Sol. Cells*, 2007, **91**, 1749–1754; (*b*) G.-W. Lee, D. H. Kim, M. J. Ko, K. K. Kim and N.-G. Park, *Sol. Energy*, 2010, **84**, 418–425.

17 Y. Kawamura, H. Mashiyama and K. Hasebe, *J. Phys. Soc. Jpn.*, 2002, **71**, 1694–1997.

18 A. J. Frank, N. Kopidakis and J. van de Lagemaat, *Coord. Chem. Rev.*, 2004, **248**, 1165–1179.